A hybrid method for computing forces on curved dislocations threading to free surfaces

M. Tang, W. Cai, G. Xu, V. V. Bulatov

June 10, 2005

A hybrid method for computing forces on curved dislocations threading to free surfaces

Meijie Tang[*]†, Wei Cai‡, Guanshui Xu§, Vasily V. Bulatov†

†Lawrence Livermore National Laboratory, Livermore, CA 94551, USA
‡Mechanical Engineering Dept., Stanford University, Stanford, CA 94305, USA
§Mechanical Engineering Dept., University of California, Riverside, CA 92521, USA

Abstract

Dislocations threading to free surfaces present a challenge for numerical implementation of traction-free boundary conditions. The difficulty arises when canonical (singular) solutions of dislocation mechanics are used in combination with the Finite Element or Boundary Element (Green's function) methods. A new hybrid method is developed here in which the singular part and the non-singular (regular) part of the image stress are dealt with separately. A special analytical solution for a semi-infinite straight dislocation intersecting the surface of a half-space is used to account for the singular part of the image stress, while the remaining regular part of the image stress field is treated using the standard Finite Element Method. The numerical advantages of such regularization are demonstrated with examples.

Keywords: Threading dislocations; Dislocation dynamics; Image stress; Thin film

1 Introduction

The last decade has witnessed the emergence of Dislocation Dynamics (DD) simulations as a powerful computational approach for studying mechanical behaviour of materials based on the fundamental dislocation mechanisms (Kubin and Canova, 1992; Tang et al., 1998; Zbib et al., 1998; Ghoniem et al., 2000). Direct simulations of dislocation behavior in thin films and microelectronic devices is one of the appealing applications of this, still relatively new approach (Schwarz, 1999; Wang et al., 2004). General aspects of the DD method have been widely described in the literature (Weygang et al., 2002; Bulatov et al., 2001). In brief, the DD simulations track the motion of dislocation lines that are usually represented by connected line segments. The dislocations move in response to forces produced by external loads, other dislocations, and various other defects, e.g. free surfaces or grain boundaries. The major computational expense of DD simulations is the evaluation of forces due to stress produced by the dislocation segments. To save the computational effort this stress is computed using the simple (canonical) solutions for dislocations in an infinite elastic solid body (Hirth and Lothe, 1982; Devincre, 1995).

In the case of a finite elastic body with free surfaces, the stress computed from the canonical solutions makes up for non-zero tractions at the free surfaces. These non-zero tractions need to be corrected in order to satisfy the free surface boundary condition. The

---

[*] Corresponding author. Email address: tang7@llnl.gov (Meijie Tang).

image stress is defined as the extra stress produced by such a correction. In the Green's function (Boundary Element) approach, distributed forces are applied to the surface in order to cancel the spurious tractions associated with the canonical solutions. The stress induced by these extra forces is then computed using the appropriate Green's function for the half-space (Fivel et al., 1996; Liu et al., 2000). Likewise, Finite Element Method (FEM) has been used to enforce the traction-free boundary conditions in DD simulations (Weygang et al., 2002; Martinez and Ghoniem, 2002; Tang et al., 2003). Although different, these two approaches rely on meshes in their numerical implementation.

The FEM approach has been shown to be ineffective when treating a dislocation segment that intersects with a surface (Tang et al. 2003). The efficiency and the accuracy of the method were largely limited by the need to cancel the spurious singular stress produced by the canonical solution at the intersection point of the dislocation line and the surface. By refining the mesh, the results showed improvement but the convergence to an exact solution was slow. A major difficulty in trying to improve the accuracy by mesh refinement is that the number of mesh points required for the numerical solution to converge is often too large for practical implementation, especially when multiple threading dislocations are considered. Further difficulty arises when threading dislocations move and overlap with the Gaussian integration points causing numerical instabilities. The use of adaptive meshes to track the dislocation threading points is possible but cumbersome. Through extensive numerical experimentation, Tang et al. (2003) concluded that the standard FEM is not a practical method to treat multiple threading dislocations in large-scale DD simulations due to a high computational burden associated with meshing.

In this paper, we describe an improved hybrid approach to effectively calculate the image stress associated with threading dislocations in finite elastic bodies. The hybrid method is developed where the singular part of the stress field associated with a threading dislocation is accounted for using a known analytical solution for a semi-infinite straight dislocation intersecting the free surface of a half-space. The numerical advantage of this trick is that the remaining, non-singular part of the image stress field can be accurately treated with much coarser FEM meshes. In the subsequent section, we briefly review the Dislocation Dynamics and the Finite Element Method used in this work. The new hybrid method is presented in section 3 and some examples of its application are given in section 4. Finally, discussions and conclusions are given in section 5.

2 Existing Methods

Dislocation Dynamics

In our Dislocation Dynamics simulations, the dislocation lines are represented by straight segments connecting a set of nodes. The nodal position $\mathbf{r}_i$ and the Burgers vectors of the segments are the degrees of freedom in the model (Cai et al., 2004; Bulatov et al., 2004). The driving force $\mathbf{f}_i$ on every node is computed at the beginning of every time step of a DD simulation. In most cases of interest, the effect of inertia on dislocation motion can be ignored so that the dislocation equation of motion is first-order, i.e., the

instantaneous velocities of the nodes are completely determined by their driving forces through a mobility function (Cai and Bulatov, 2004). In the following, we discuss the calculation of nodal forces and velocities in some detail.

In our model, the dislocation lines are represented as straight segments connecting the nodes. Each node can have an arbitrary number of segments connected with the neighboring nodes. The force on a node is fully defined by the Peach-Koehler (PK) forces on the dislocation segments connected to the node (Cai, 2001). The PK force on a dislocation segment at point $\mathbf{x}$ is

$$\mathbf{f}^{PK}(\mathbf{x}) = \boldsymbol{\sigma}(\mathbf{x}) \cdot \mathbf{b} \times \boldsymbol{\xi}(\mathbf{x}) \tag{1}$$

where $\boldsymbol{\sigma}(\mathbf{x})$ and $\boldsymbol{\xi}(\mathbf{x})$ are the stress tensor and the unit tangent vector at point $\mathbf{x}$ on the segment and $\mathbf{b}$ is its Burgers vector. When a virtual displacement is applied at node i, the shape change of the dislocation line is a piece-wise linear function along the dislocation segments, as shown in Fig. 1. Let us define a shape function $N_i(\mathbf{x})$ for every node i. The function is non-zero only if $\mathbf{x}$ lies on a segment connected to node i. Suppose $\mathbf{x}$ lies on segment i-j, then

$$N_i(\mathbf{x}) = \frac{\left| \mathbf{x} - \mathbf{x}_j \right|}{\left| \mathbf{x}_i - \mathbf{x}_j \right|} \tag{2}$$

i.e., $N_i(\mathbf{x})$ goes linearly from zero at node j to one at node i (see Fig. 1(b)). Therefore, the shape change of the entire dislocation line corresponding to the virtual displacement $\delta \mathbf{r}_i$ is

$$\delta \mathbf{r}(\mathbf{x}) = N_i(\mathbf{x}) \delta \mathbf{r}_i \tag{3}$$

It follows that the force on node i is

$$\mathbf{f}_i = \int_C \mathbf{f}^{PK}(\mathbf{x}) N_i(\mathbf{x}) dL(\mathbf{x}) \tag{4}$$

Because the stress field produced by dislocations has singularities right on the dislocation lines, some truncation is usually applied to avoid this singularity and to compute self-forces on the lines. For example, in Fig. 1, the stresses between segments 0-1 and 1-2, and 1-2 and 2-3 are singular on segment 1-2 (or on its end nodes). To avoid the singularity, we adopt the approach proposed by Brown (1964), in which the stress field is never computed on the segment itself. Instead, the stress is computed first on both sides of the segment on the glide plane at a distance ρ to the segment and then the average of the two stress values is used for computing the Peach Koehler force $\mathbf{f}^{PK}(\mathbf{x})$ (Schwarz, 1999). Within isotropic elasticity, the stress field produced by an arbitrary straight dislocation segment is available analytically (Hirth and Lothe, 1982).

For simplicity, we will use a linear mobility function in this study to relate nodal force to nodal velocity, i.e.,

$$\mathbf{v}_i = M\mathbf{t}_i g_i H(g_i) \tag{5}$$

$$\mathbf{t}_i = \mathbf{f}_i / |\mathbf{f}_i|$$
$$g_i = |\mathbf{f}_i| / L_i - \tau_p b \tag{6}$$

where $\mathbf{v}_i$ is the velocity of node i, M is a mobility constant, and $\mathbf{t}_i$ is the unit vector along $\mathbf{f}_i$, L_i is half of the total length of all segments connected to node i, τ_p is a minimal stress (Peierls stress) required for dislocation motion and b is the magnitude of the Burgers vector. H(x) is a step function that equals one if x>0 and equals zero if x<0. The step function guarantees that the velocity is zero when the driving force per unit length is smaller than the resistance force due to the Peierls stress.

After the nodal velocities are computed, the nodal positions are updated using a numerical integrator. For simplicity, the forward Euler integrator is used in this study, i.e.,

$$\mathbf{r}_i(t + \Delta t) = \mathbf{r}_i(t) + \mathbf{v}_i(t)\Delta t \tag{7}$$

Finite Element Method

The Finite Element Method is a standard method to solve boundary value problems in elasticity (Hughes, 2000). The FEM code used in this work relies on direct and conjugate gradient iterative solvers. The latter is considerably more efficient for large systems with thousands (or more) of elements. Regular meshes (i.e., brick) are used throughout the calculations with the mesh size ranging from 0.1 to 0.6 nm. The largest system reported here contains 10.8×10^6 elements. For simplicity, the stress field is sampled at a single Gaussian point in each element. Thus, stress in any given point in space is taken as the stress in the element in which the point resides.

In all calculations presented in this communication, we used rectangular simulation boxes with large x and y dimensions and a small z dimension. For the cases with only one free surface at the top, the zero-displacement boundary conditions were applied for all other surfaces unless otherwise noted. For the case with two free surfaces, one at the top and another at the bottom, the zero-displacement boundary conditions were applied only for the side surfaces.

3 The Hybrid Method

4

An analytical solution for the stress field of an infinite straight dislocation intersecting a free surface in a semi-infinite medium was obtained by Yoffe (1961). The original publication had several misprints that were later corrected (Shaibani and Hazzledine, 1981; Hazzledine and Shaibani, 1982). The corrected solution is used in this work. The Yoffe analytical solution ($\boldsymbol{\sigma}^y(\mathbf{r})$) is for the total stress field that can be understood as the sum of the stress of the straight dislocation in an infinite medium ($\boldsymbol{\sigma}^\infty(\mathbf{r})$) and the image stress due to the free surface ($\boldsymbol{\sigma}^{y\text{-img}}(\mathbf{r})$). Since the stress field of a dislocation segment in an infinite medium is readily available in a simple analytic form (Hirth and Lothe, 1982; Devincre, 1995), the image stress tensor is simply $\boldsymbol{\sigma}^{y-\text{img}}(r) = \boldsymbol{\sigma}^y(r) - \boldsymbol{\sigma}^\infty(r)$. This image stress tensor will be used for the calculation of the nodal force due to the free surface, as discussed in section 2.

To validate our numerical implementation of the Yoffe image stress solution, we compare it with an FEM calculation in a rectangular solid (Fig. 2). In this calculation, only the top surface is assumed to be free of tractions. Zero displacement boundary conditions are applied at four side surfaces. To minimize possible artifacts, a fixed surface traction boundary condition is used at the bottom surface with the tractions computed from the Yoffe analytical solution. This was shown to provide more accurate results for the stress field close to the bottom surface. As an additional test for consistency, we verified that, in the case when a dislocation is perpendicular to the free surface, the stress field reduces from the general Yoffe solution to one found by Honda (1979).

The Yoffe analytical solution is directly applicable only in an idealized situation where the dislocation is straight and semi-infinite. For DD simulations, it is necessary to handle curved dislocations. Typically, a curved dislocation in the DD simulation is represented by piece-wise connected dislocation segments as shown in Fig. 3(a). As a source of stress field, such a dislocation configuration can be regarded as a superposition of the configuration in Fig. 3(b) containing the Yoffe dislocation and the configuration in Fig. 3(c) in which the dislocation never emerges at the surface. The advantage of this decomposition is that the solution for Fig. 3(b) is available analytically while the solution for Fig. 3(c) is a benign case for an FEM calculation since the surface tractions produced by the non-threading segments are finite. Thus, we have intentionally separated the image stress into two distinctly different components: one produced by singular tractions associated with the threading segment and another one produced by non-singular surface tractions associated with all non-threading segments.

A simple test case used to investigate the convergence and accuracy of the hybrid method is shown in Fig. 4. The test configuration consists of a curved semi-infinite dislocation represented by three connected segments, in a semi-infinite medium. Clearly, the hybrid method based on our "singular-nonsingular decomposition" shows nearly no mesh dependence compared to the standard FEM solution with no decomposition that shows strong mesh dependence. The accuracy of the results from the standard FEM is considerably lower, down to the smallest mesh size used in the calculations. It turns out that the major contribution to the forces on node 0 and node 1 come from the image stress

of the segment intersecting the free surface. In the hybrid method, this contribution is computed using the Yoffe analytical solution and is essentially mesh-independent, whereas the standard FEM calculation shows strong mesh dependence due to the singularity of the surface tractions associated with the threading segment. Although not visible in the figure, there is a very weak dependence on the mesh size still remaining in the hybrid method. This comes from the non-singular image stresses due to the other two non-threading segments. Over the range of mesh size considered, the magnitudes of the forces on nodes 0 and 1 change by 0.3% and 0.7%, respectively, for the hybrid method.

So far, the hybrid method was applied to a half-space with only one free surface. It can be further generalized to a finite elastic body with multiple free surfaces, e.g. a thin film or a multi-faced polyhedron such as shown in Fig. 5. Similar to what has been already discussed, there will be numerical problems due to the singular traction force on surface 1 if one uses the standard FEM. It is not immediately obvious that it is possible to take advantage of the Yoffe solution in the situation described in Fig. 5. This is because the Yoffe solution satisfies the traction free boundary condition only for the case of a semi-infinite straight dislocation threading to a planar surface bounding a half-space. Furthermore, it appears that the superposition described in Fig. 3 will exacerbate the difficulties by producing singularity on surface 3 and additional unbalanced tractions on the other surfaces. This, seemingly difficult, situation can in fact be handled. Below we show how the Yoffe solution, combined with linear superposition, leads to a hybrid DD/FEM framework in which singular surface tractions normally associated with the threading dislocations do not appear on any of the surfaces.

Consider again a segment AB terminating at a free surface as shown in Fig. 5. Its stress field can be written as

$$\boldsymbol{\sigma}_{AB} = \boldsymbol{\sigma}_{AB}^{\infty} + \boldsymbol{\sigma}^{img} \tag{8}$$

where $\boldsymbol{\sigma}_{AB}$ is the stress field in the finite elastic body, $\boldsymbol{\sigma}_{AB}^{\infty}$ is the stress field of segment AB in an infinite elastic body and $\boldsymbol{\sigma}^{img}$ is the image stress field required to satisfy the traction-free boundary conditions. Again, if the standard FEM is used to solve for the boundary condition, singular traction forces will be encountered on surface 1. Thus, we try to use the Yoffe image stress solution at surface 1 for the threading segment. One way to do it is to add the Yoffe image stress to the stress produced by segment AB everywhere in the finite body

$$\boldsymbol{\sigma}_{AB} = \boldsymbol{\sigma}_{AB}^{\infty} + \boldsymbol{\sigma}_{AB'}^{y\text{-img}} + \boldsymbol{\sigma}^{corr-img}. \tag{9}$$

The new image stress $\boldsymbol{\sigma}^{corr-img}$ required to cancel the tractions on the surfaces can be found by solving the following boundary condition

$$\mathbf{t} = -(\boldsymbol{\sigma}_{AB}^{\infty} + \boldsymbol{\sigma}_{AB'}^{y-img}) \cdot \mathbf{n} , \tag{10}$$

6

where **n** is the unit normal vector (each surface has its own normal vector **n**). Since both stress terms in the above equation are finite on all surfaces except surface 1, the boundary conditions in Eqn. (10) are non-singular on those surfaces. At the same time, Eqn. (10) can be rewritten by adding and subtracting stress $\boldsymbol{\sigma}_{BB'}^{\infty}$ due to the semi-infinite segment BB'. Recognizing that on surface 1 the Yoffe solution holds

$$(\boldsymbol{\sigma}_{AB}^{\infty} + \boldsymbol{\sigma}_{BB'}^{\infty} + \boldsymbol{\sigma}_{AB'}^{y-img}) \cdot \mathbf{n} = \mathbf{0} \; , \tag{11}$$

we arrive at our final result for the boundary condition to be used to solve for the image stress $\boldsymbol{\sigma}^{corr-img}$

$$\begin{aligned} \mathbf{t}_1 &= -\boldsymbol{\sigma}_{B'B}^{\infty} \cdot \mathbf{n}_1 \\ \mathbf{t}_i &= -(\boldsymbol{\sigma}_{AB}^{\infty} + \boldsymbol{\sigma}_{AB'}^{y-img}) \cdot \mathbf{n}_i, \; i = 2, 3, 4 \end{aligned} \tag{12}$$

Since segment B'B does not intersect surface 1, segment AB intersects only surface 1, and the Yoffe image stress $\boldsymbol{\sigma}_{AB'}^{y-img}$ is finite on surfaces 2, 3 and 4, the traction forces in Eqn. (12) are non-singular on all the surfaces.

In practice a DD simulation can involve multiple dislocation segments intersecting different free surfaces. By using Eqn. (9) for each threading segment and adding contributions from the boundary condition in Eqn. (12), it is straightforward to obtain the combined image stress due to all threading segments. For segments that do not intersect the free surfaces, the image stress is obtained using the standard FEM.

4 Examples of Application

This section discusses two examples of the application of the hybrid method presented above. Both examples are related to dislocation behavior in small systems. The first one examines the stress fields produced by a single dislocation threading across a thin film. The second example is a dynamic simulation of the behavior of a dislocation half-loop in a half-space bounded by a planar surface. In both cases, we use the Yoffe solution to obtain accurate image corrections for stress and the PK forces on dislocations. In these simulations, the hybrid method allows us to use rather coarse FEM meshes keeping the overall cost of the FEM calculations small compared to the DD part of the problem. To highlight the significance of the image effects, we compare the fully corrected results with the corresponding cases where no image correction is performed.

The first example is a calculation of the stress fields produced by a single screw/edge dislocation in a film. The dislocation is straight and threads along z direction, perpendicular to the top and the bottom free surfaces where the traction-free boundary condition is applied. To gauge the importance of the image stress to dislocation behavior in thin films, we note that the Peach-Koehler interaction force per unit length between a pair of parallel screw dislocations is $\mathbf{f} = b(\sigma_{yz}\mathbf{i} - \sigma_{xz}\mathbf{j})$, where $\mathbf{i}$ and $\mathbf{j}$ are two unit vectors along x and y direction respectively. Fig. 6 shows contour plots of the stress component

7

σ_{xz} (in the unit of shear modulus μ) in the middle plane of the simulation box. The results are similar for σ_{yz} component. From (a) to (c), the film thickness changes from 2 nm, to 4 nm to infinity. As seen clearly, the stress field is confined in a local region around the dislocation when the image correction is employed. The size of the region where stress is concentrated scales with the film thickness. This means that the elastic interaction among screw dislocations is significantly modified in the films where it becomes short ranged[†]. Also shown in Fig. 6 are the stress contours for a threading screw segment terminating at the surfaces in a 4 nm and 2 nm films but without any image correction. Although the contours show certain stress confinement, the traction-free boundary condition is clearly violated at the top and bottom surfaces.

The results for the edge dislocation are qualitatively different. The Peach-Koehler force per unit length between a pair of parallel edge dislocations is $\mathbf{f} = b(\sigma_{xy}\mathbf{i} - \sigma_{xx}\mathbf{j})$. Fig. 7 shows the contour plots of stress component σ_{xy} in the middle plane of the simulation box. The results are similar for σ_{xx} component. Although the elastic interaction between a pair of edge dislocations in a film is modified relative to an infinite solid, its qualitative features remain the same (compare (a) and (b) with (c)). Furthermore, the contours are much less dependent on the film thickness compared to the screw case. Also shown are the stress contours of a threading edge segment terminating at the surfaces computed without any image stress correction. Its qualitative features in this case are different from that in the infinite solid. The stress field appears to be over confined.

The second application concerns the stability of a dislocation half-loop inserted just below a free surface with normal vector along [001] at z = 0. The half-loop initially consists of 3 segments, i.e., two edges of length 200b and one screw of length 283b. Its Burgers vector along [110] is parallel to the surface. Somewhat below the half-loop at z = -300b, a relatively long straight screw dislocation with an opposite Burgers vector runs parallel to the free surface over the total length of 707b. The two ends of this dislocation are fixed. No cross-slip is allowed so that the segments of both dislocations can move only in the $(1\bar{1}0)$ slip plane. The initial arrangement is such that the half-loop and the straight line attract each other elastically. Counteracting this attraction is the image stress from the free surface that pulls the half-loop towards it. In the simulations, the dislocation mobility constant M is the same for both screw and edge (the results are insensitive to the choice of M) and the Peierls stress is $1.5 \times 10^{-4}\mu$. The simulation is first performed using the hybrid DD/FEM method. Due to the image stress, the half-loop shrinks and disappears at the surface following some initial relaxation due to the line tension. The snapshots of the sequence of events are shown in Fig. 8(a). Next, the same simulation is performed ignoring the image stress correction. After some initial relaxation, the half-loop and the screw below move towards each other and recombine. In this case, the attraction between them is strong enough to cause recombination. The snapshots of this sequence of events are shown in Fig. 8(b).

[†] A similar observation was made by Eshelby and Stroh (1951).

Additional simulations are performed to elucidate the effect of the Peierls stress on the behavior of the dislocation half-loop. When the Peierls stress is increased by a factor of five, the behavior remains qualitatively similar to that just discussed. At a larger Peierls stress, both the half-loop and the screw become more constrained. When the Peierls stress is increased by a factor of ten, the half-loop is still found to shrink and disappear at the free surface. However, in the case without the image stress correction, the half-loop remains right below the free surface with a small curvature while the screw dislocation below did not show any significant response.

5 Summary

In this paper, we presented an efficient method for computing the image stresses produced by an arbitrary dislocation arrangement in a finite isotropic elastic body. The method is based on a special treatment of the singular part of the image stress near the points where the dislocations terminate at the free surfaces. The hybrid method achieves a high accuracy and computational efficiency by dispensing with the need for excessive mesh refinement near the termination points. At present, our approach relies on the standard framework of the singular continuum theory of dislocations. Further development is underway to extend this approach to a non-singular version of the continuum theory (Cai et al., 2005).

The applications performed in this paper are preliminary. But they demonstrate the importance of the image stress in small systems. In the case of a screw dislocation in a thin film, the image stress is found to alter the characteristic interaction between screws from the long ranged interaction characteristic of the bulk crystals to a short ranged interaction. In the case of a dislocation half-loop below a flat surface, the image stress is shown to significantly attract the loop leading to loop disappearance. Further calculations are underway to study the effect of image stresses on dislocation behavior in small systems with complex geometries.

References

Brown, L. M., The Self-stress of Dislocations and the Shape of Extended Nodes, Philos. Mag. **10**, 441 (1964).

Bulatov, V. V., Tang, M., and Zbib, H. M., 2001. Dislocation Plasticity from Dislocation Dynamics. MRS Bulletin **26**, 191.

Bulatov, V. V., Cai, W., Fier, J., Hiratani, M., Pierce, T., Tang, M. Rhee, M., Yates, K., and Arsenlis, A., 2004. Scalable line dynamics of ParaDiS, SuperComputing, p.19. online at http://www.sc-conference.org/sc2004/schedule/pdfs/pap206.pdf.

Cai, W., 2001. *Atomistic and Mesoscale Modeling of Dislocation Mobility,* Ph. D. Thesis, Massachusetts Institute of Technology.

Cai, W., Bulatov, V. V., Pierce, T. G., Hiratani, M., Rhee, M. Bartelt, M., and Tang, M., 2004. Massively-Parallel Dislocation Dynamics Simulations, in *Solid Mechanics and Its Applications,* H. Kitagawa, Y. Shibutani , eds., vol. 115, p.1, Kluwer Academic Publishers.

Cai, W., and Bulatov, V. V., 2004. Mobility Laws in Dislocation Dynamics Simulations, Mater. Sci. Eng. A, 387-389, 277.

Cai, W., Arsenlis, A., Weinberger, C. R., and Bulatov V. V., 2005. A non-singular continuum theory of dislocations. Submitted to J. Mech. Phys. Solids.

Devincre, B., 1995. Three Dimensional Stress Field Expressions for Straight Dislocation Segments. Solid Stat. Comm. **93,** 875.

Eshelby, J. D., and Stroh, A. N., 1951. Dislocations in Thin Plates. Phil. Mag. **42**, 1401.

Fivel, M. C., Gosling, T. J., and Canova, G. R., 1996. Implementing image stresses in a 3D dislocation simulation. Modeling Simul. Mater. Sci. Eng. **4,** 581.

Ghoniem, N. M., Tong, S. –H., and Sun, L. Z., 2000. Parametric dislocation dynamics: A thermodynamics-based approach to investigations of mesoscopic plastic deformation. Phys. Rev. B **61,** 913.

Hazzledine, P. M., and Shaibani, S. J., 1982. The Behaviour of Dislocations Near a Free Surface. ICSMA, ed. R. C. Gifkins, Pergamon Press, p.45.

Hirth, J. P., and Lothe, J., 1982. *Theory of dislocations*, 2nd Ed., Wiley, New York.

Honda, K., 1979. Dislocation Walls Consisting of Double Arrays in White Tin Single Crystals. Jap. J. Appl. Phys. **18,** 215.

Hughes, T. J. R., 200. *The Finite Element Method: linear static and dynamic finite element analysis* (Dover Publications Inc., Mieola, New York).

Kubin, L. P. and Canova, G. R., 1992. The modelling of dislocation patterns. Scripta Metall. Mater. **27** 957.

Liu, X. H., Ross, F. M., and Schwarz, K. W., 2000. Dislocated Epitaxial Islands. Phys. Rev. Lett. **85,** 4088.

Martinez, R., and Ghoniem, N. M., 2002. The Influence of Crystal Surfaces on Dislocation Interactions in Mesoscopic Plasticity: A Combined Dislocation Dynamics-Finite Element Approach. J. Comp. Meth. Eng. Sci., CMES **3(2),** 229.

Shaibani, S. J., and Hazzledine, P. M., 1981. The displacement and stress fields of a general dislocation close to a free surface of an isotropic solid. Phil. Mag. **44,** 657.

Schwarz, K. W., 1999. Simulation of dislocations on the mesoscopic scale. I. Methods and examples. J. Appl. Phys. **85,** 108.

Tang, M., Kubin, L. P., and Canova, G. R., 1998. Dislocation Mobility and the Mechanical Response of B.C.C. Single Crystals: a mesoscopic approach. Acta Mater. **46,** 3221.

Tang, M., Xu, G., Cai, W., and Bulatov, V. V., 2003. Dislocation image stresses at free surfaces by the finite element method, in *Thin Film Stresses and Mechanical Properties,* S. G. Corcoran, Y-C. Joo, N. R. Moody, and Z. Suo, eds., Materials Research Society, Warrendale, PA, **795,** U2.4.

Wang, Z., McCabe, R. J., Ghoniem, N. M., LeSar, R., Misra, A., and Mitchell, T. E., 2004. Dislocation motion in thin Cu foils: comparison between computer simulations and experiment. Acta Mater. **52**, 1535.

Weygang, D., Friedman, L. H., Van der Geissen, E., and Needleman, A., 2002. Aspects of boundary-value problem solutions with three-dimensional dislocation dynamics. Modeling Simul. Mater. Sci. Eng. **10**, 437.

Yoffe, E. H., 1961. A dislocation at a Free Surface. Phil. Mag. **6,** 1147.

Zbib, H. M., Rhee, M., and Hirth, J. P., 1998. On Plastic Deformation and the Dynamcis of 3D Dislocations. Int. J. Mech. Sci. **40,** 113.
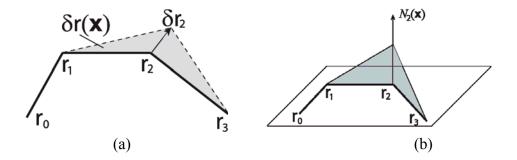
Fig. 1. The driving force on node 2 is the weighted average of the Peach-Koehler force over segments 1-2 and 2-3. (a) A virtual displacement of node 2 by $\delta\mathbf{r}_2$ causes segments 1-2 and 2-3 to sweep an area consisting of two triangles (shaded). (b) The shape function or "weighting function" $N_2(\mathbf{x})$ for the PK force on segments 1-2 and 2-3 varies linearly from 1 at node 2 to 0 at its two neighbor node 1 and 3.
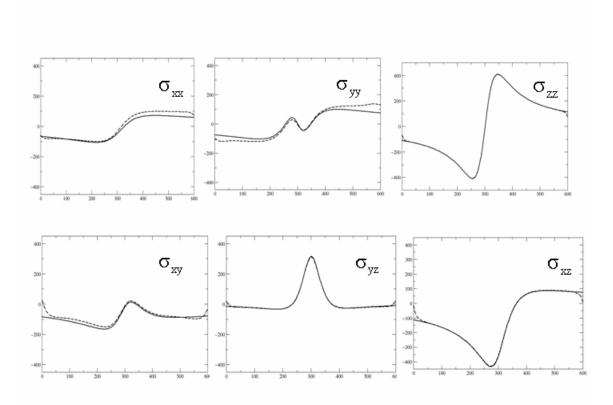
Fig. 2. Six components of the image stress of a semi-infinite mixed dislocation at an inclined angle to the surface of a half-space. The solid lines are obtained using the Yoffe solution for the image stress while the dashed lines are obtained by straightforward FEM calculations. In the FEM calculations, the simulation box is rectangular with x, y and z dimensions being 60, 60, and 6 nm respectively. The free surface is located at z = 6 nm. The dislocation line is at 5 degrees to z axis along [001], and its Burgers vector is along [111]. The FEM mesh element is a cube with 0.2 nm on each side. The comparison is performed along the line parallel to y axis and defined by x=30 nm and z=0.6 nm.
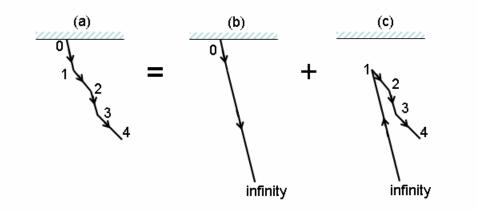
Fig. 3. Decomposition and superposition used to formulate the hybrid method are illustrated schematically for a half-space with only one free surface. As a source of stress, an arbitrarily shaped dislocation (a) terminating at the free surface is viewed here as a sum of two configurations, i.e., (b) and (c). The Yoffe solution applies directly to (b) and the standard FEM is used to calculate the image stress for (c).
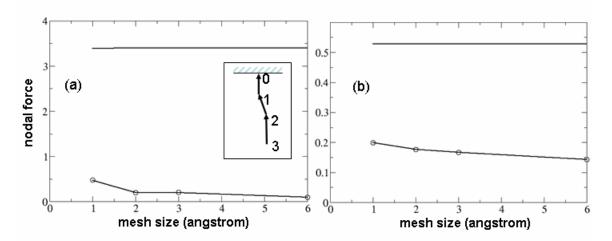
Fig. 4 A three-segment configuration (shown in the inset) is used to test the performance of the hybrid method. The lengths of the segments are 2 nm, 2 nm, and infinity for segments 0-1, 1-2, and 2-3, respectively. The angle between the middle segment 1-2 and the z axis is 30 degrees. The burgers vector is [111] and all segments are in $(1\bar{1}0)$ plane. The simulation box is rectangular with x, y, and z dimensions 30, 30 and 12 nm, respectively. The nodal force on nodes 0 and 1 are calculated using both the hybrid method and the standard FEM. The magnitude of the nodal force is shown in (a) for node 0 and in (b) for node 1. The solid lines at the top of each plot are obtained by the hybrid method and the lines with circles at the bottom are obtained using the standard FEM. The nodal force is in the unit of μb^2.
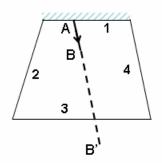
15

Fig. 5. A finite segment AB in a finite elastic body (polyhedron) is extended to infinity (marked by B'). The Yoffe solution applies to surface 1 only, whereas the image stress associated with all other surfaces is obtained using the standard FEM to enforce the zero-traction boundary condition. The hybrid method is not limited to polyhedrons. It can be applied to a generally shaped finite body.
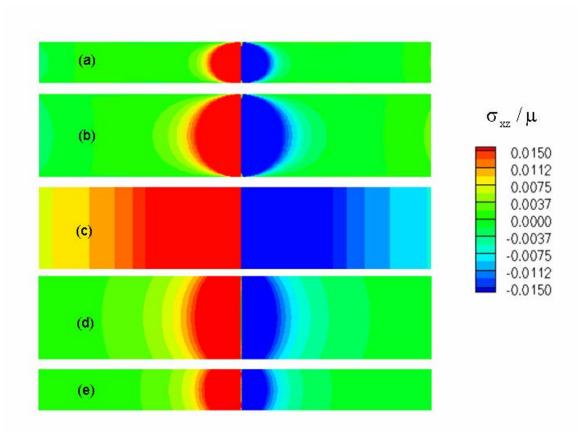
Fig. 6. The stress contours computed for a single screw dislocation. The simulation box is 20 nm along x and y directions. The dislocation lies along z direction and its Burgers vector is along [001]. The stress contours are computed in the middle plane at x = 10 nm. (a) and (b) show the stress contours in 2 nm and 4 nm films with the image stress corrections obtained by the hybrid method while (c) shows the stress contours due to an infinite screw dislocation. (d) and (e) show the stress contours of a finite screw segment terminating at the free surfaces in 4 nm and 2 nm films, but without the image stress correction.
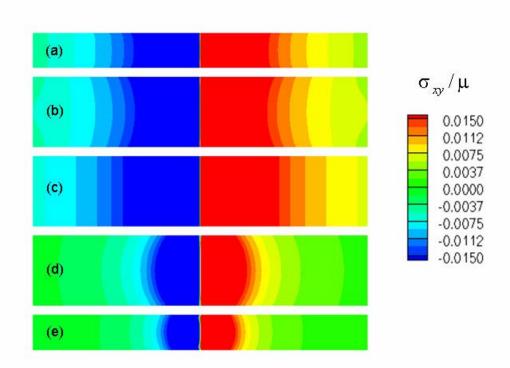
Fig. 7. The stress contours computed for a single edge dislocation. The simulation box is 20 nm along x and y directions. The dislocation lies along z direction and its Burgers vector is along [100]. The stress contours are computed for the middle plane at y = 10 nm. (a) and (b) show the stress contours in 2 nm and 4 nm films with image stress corrections computed by the hybrid method while (c) shows the stress contour of an infinite edge dislocation. (d) and (e) show the stress contours of a finite edge segment terminating at the free surfaces in 4 nm and 2 nm films, but without any image stress correction.
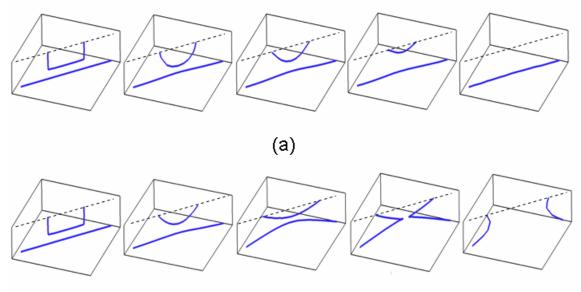
Fig. 8. A series of snapshots illustrating the time sequences observed in the DD simulations of a dislocation half-loop and a straight dislocation under a free surface. From beginning to end (left to right), the half-loop relaxes its shape while at the same time interacting with the dislocation lying below. The dashed line indicates where the free surface is. The normal to the free surface is [001] and the Burgers vectors of the half-loop and the straight dislocation are [110] and [$\bar{1}\,\bar{1}\,0$], respectively. All dislocation segments are allowed to move only in $(1\,\bar{1}\,0)$ glide plane. The dislocation lying below has its two ends fixed in space. In (a), the simulation is performed using the hybrid method with the full image stress correction enabled. The half-loop is attracted to the dislocation below and to the free surface above simultaneously. In the end, the image stress due to the free surface prevails making the half-loop shrink and disappear at the surface. In (b), the simulation is performed without any image stress correction. After some initial relaxation, the half-loop and the dislocation below attract each other and recombine.